Supporting Information

Detection of Cu(II) and NO by 'on-off' aggregation in Poly(Aryl Ether) Dendron Derivatives

*Chanchal Agarwal and Edamana Prasad**
Department of Chemistry, Indian Institute of Technology Madras, Chennai 600 036, India
Email: pre@iitm.ac.in

Contents **Page Number**

1. Synthetic procedure for model compound

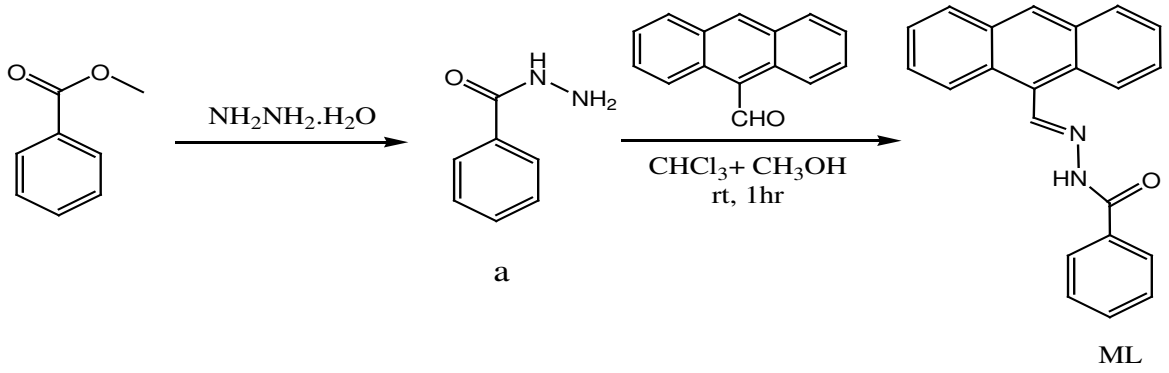

a

ML

1.1 **Synthesis of MLNHNH$_2$ (a)**

Compound ML-COOCH$_3$ (2.5 g, 0.018 mole) and hydrazine monohydrate (45 mL, 0.9 mole) were dissolved in MeOH (12 mL) and THF (6 mL). The reaction mixture was stirred at 70 C for 12 hours. After the completion of the reaction, the reaction mixture was allowed to cool to room temperature. The volatiles were removed under reduced pressure. The residue was washed with water to get pure white product (2.3 g, 92 %); **^{1}H NMR (400 MHz, CDCl$_3$) δ:** 4.088 (s, N*H*, 2H), 7.34-7.69 (m, Ar*H*, 5H), 7.72 (S, N*H,* H); **^{13}C NMR (100 MHz, DMSO-d$_6$) δ:** 126.99, 128.83, 132, 132.75, 168.85; **HRMS (ES+)**: *m/z* Calcd for $C_7H_8N_2O$: 136.15 found: 137.07 $[M+H]^+$; m. p. 94 ˚C.

1.2 **Synthesis of ML**

A solution of 9-anthracene carboxaldehyde (0.99 g, 0.0048 mole) in methanol was added dropwise to a $CHCl_3$ solution of compund **a** (0.653 g, 0.0048 mole). The mixture was stirred for 1 hour and the resulting solid was dried under vacuum to yield ML (0.96 g, 97 %).**^{1}H NMR (400 MHz, DMSO-d$_6$) δ**: 7.58-7.65 (m, Ph*H* & An*H*, 7H), 8.02 (d, *J* =7 Hz, An*H*, 2H), 8.17 (d, *J*=8Hz, An*H*, 2H), 8.73 (d, *J*=3.6Hz, AnH, 3H), 9.64 (s, C*H*=N, 1H), 12.14 (s, N*H*, 1H) ; **^{13}C NMR (100 MHz, DMSO-d$_6$) δ:** 163.90, 147.59, 133.55, 132.48, 131.36, 131.31, 130.22, 130.022, 129.43, 129.10, 128.61, 128.46, 128.06, 127.71, 126.08, 125.39, 125.30, 125.14; **HRMS (ES+)**: *m/z* Calcd for $C_{22}H_{16}N_2O$: 324.38 found: 325.13 $[M+H]^+$; m. p. 234 ˚C.

2. UV-vis absorption spectra of compound ML, AB2G1-L, AB2G2-L and AB3G2-L in presence of various metal ions (M)

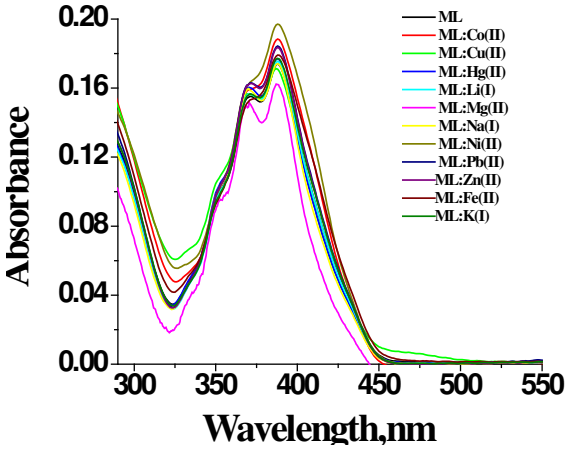

M-ML

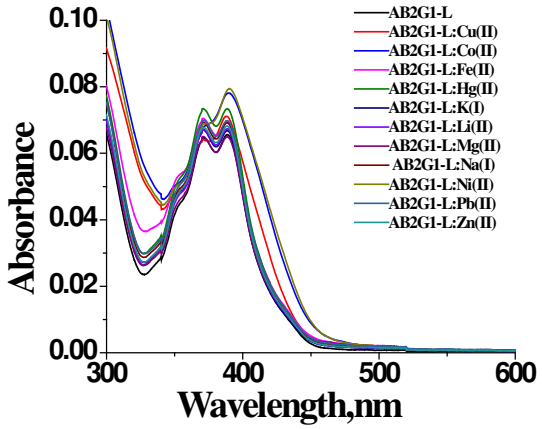

M-AB2G1-L

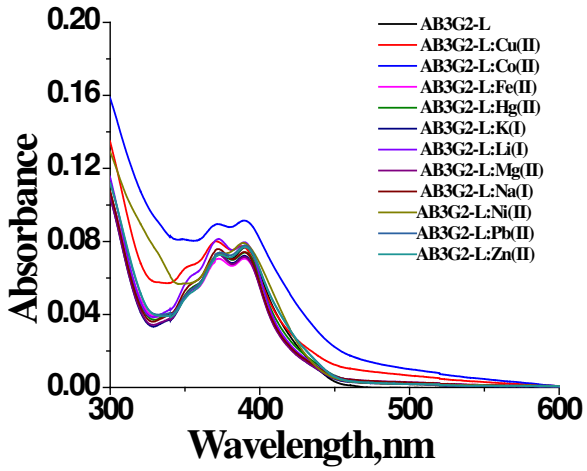

M-AB2G2-L

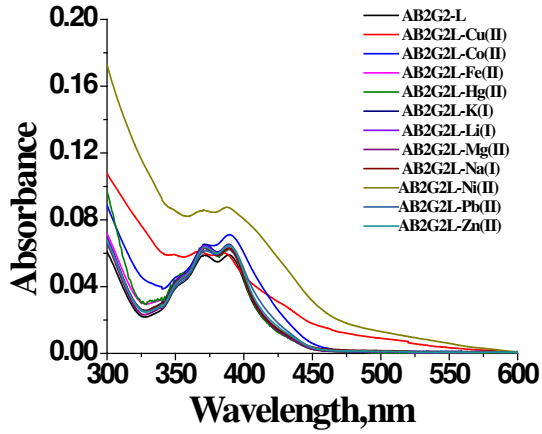

M-AB3G2-L

Figure S1: UV-vis absorption spectra of compound ML, AB2G1-L, AB2G2-L and AB3G2-L (7.5μM) in the presence of various metal ions (M) (7.5μM each) in acetonitrile at room temperature.

3. Steady state fluorescence spectra of compound ML, AB2G1-L, AB2G2-L and AB3G2-L in presence of various metal ions

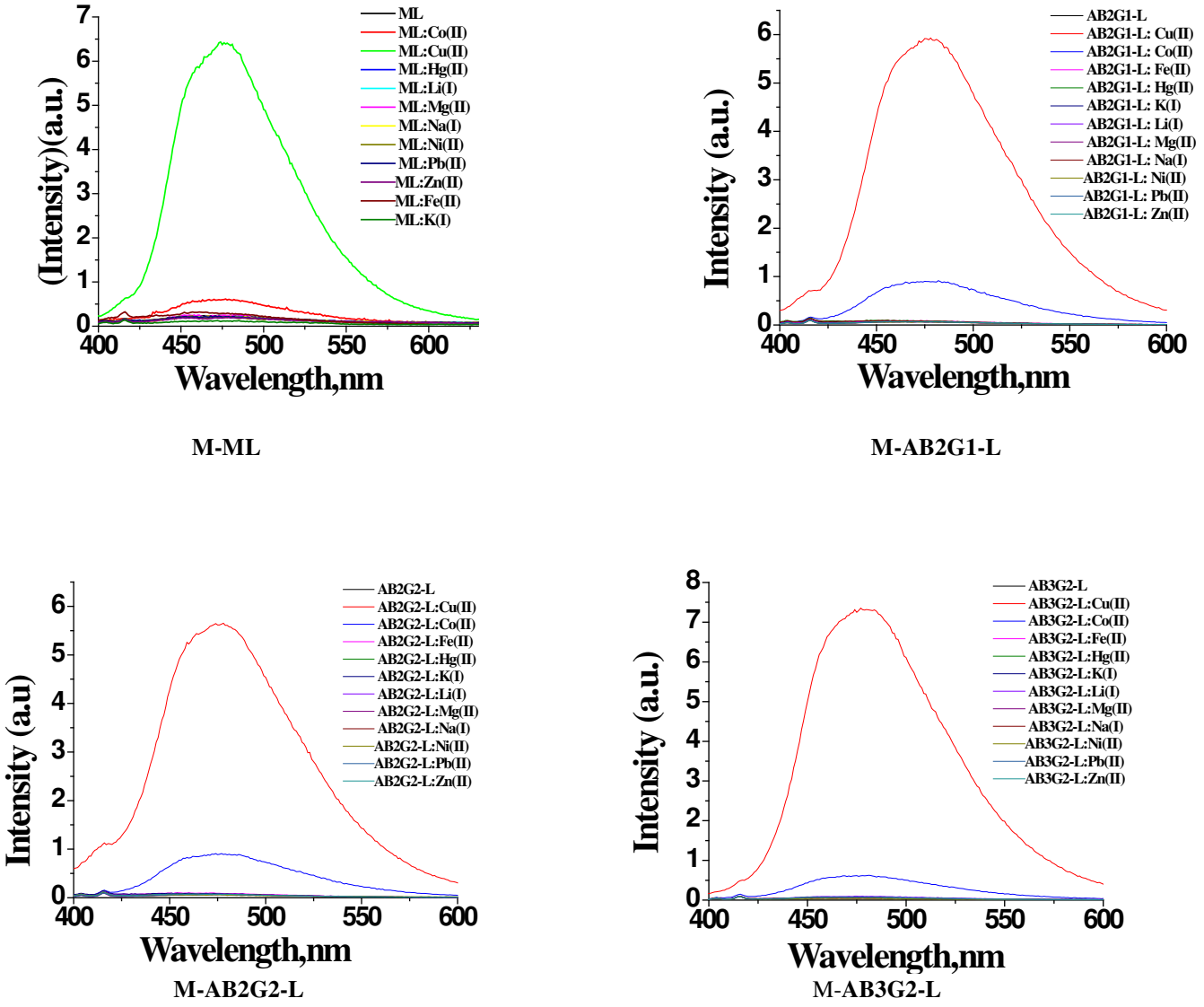

Figure S2: The steady state emission spectra of ML, AB2G1-L, AB2G2-L and AB3G2-L (7.5μM) in the presence of various metal ions (M) (7.5 μm each) in acetonitrile. λ_{ex} was 370 nm.

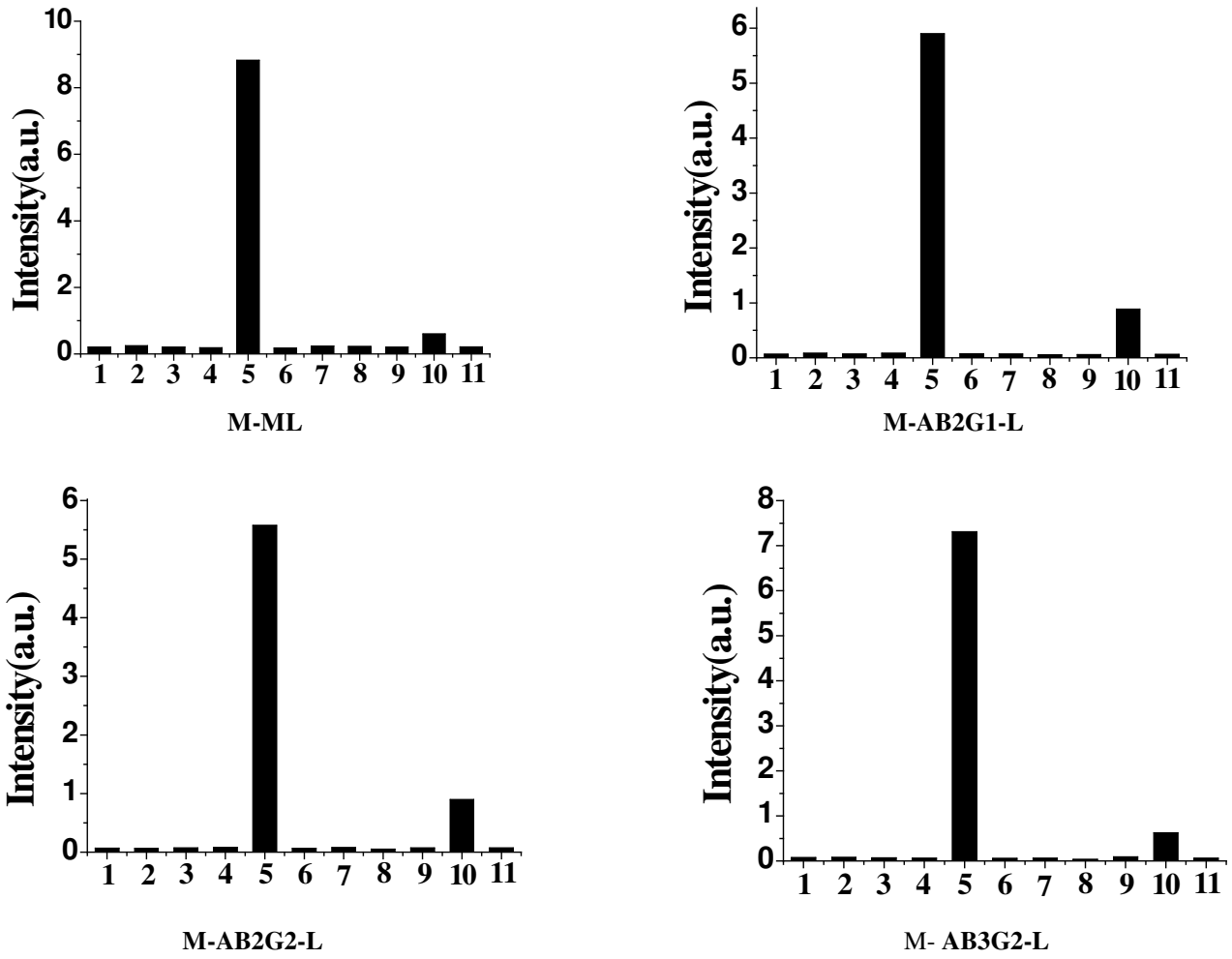

Figure S3: The steady state emission change at 480 nm from AB3G1-L (7.5μM) upon addition of 1 equiv cation (M) of interest: 1, Li(I); 2, Na(I); 3, K(I); 4, Zn(II); 5, Cu(II); 6, Mg(II); 7, Ni(II); 8, Pb(II); 9, Hg(II); 10, Co(II); 11, Fe(II) in acetonitrile. λ_{ex} was 370 nm.

4. **Jobs plot**

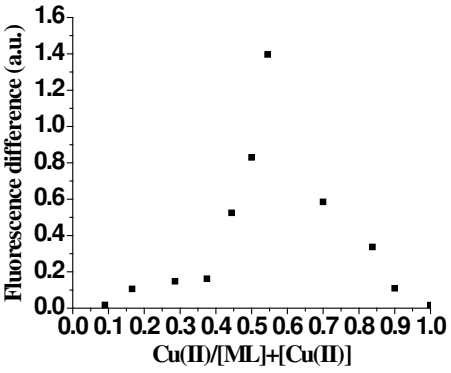

Cu(II)-ML

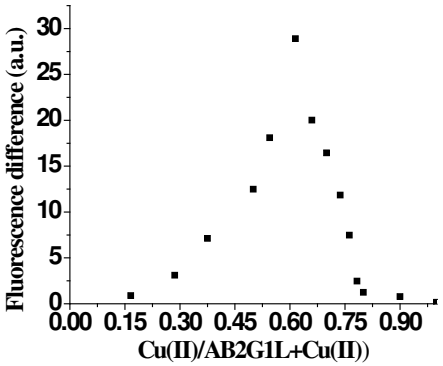

Cu(II)-AB2G1-L

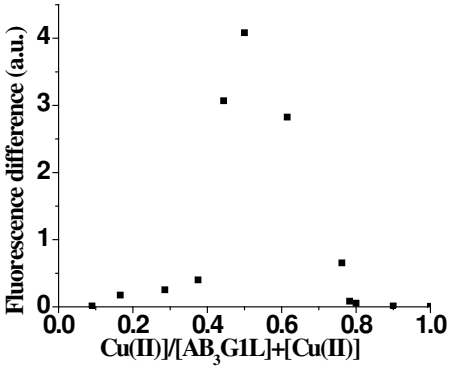

Cu(II)-AB3G1-L

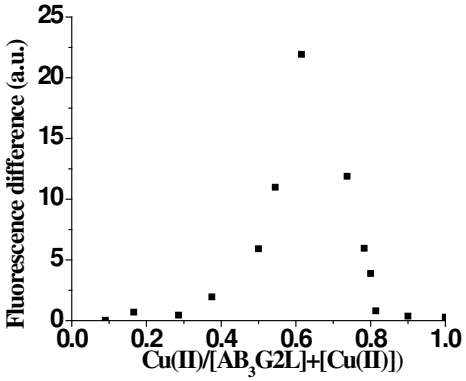

Cu(II)-AB2G2-L

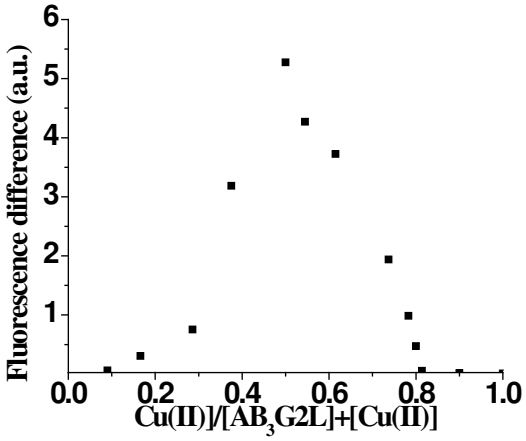

Cu(II)-AB3G2-L

Figure S4: Job's plot of a 1:1 complex of ML, AB2G1-L, AB3G1-L, AB2G2-L and AB3G2-L and Cu(II), where the difference in fluorescence intensity at 481 nm is plotted against the mole fraction of Cu(II) at constant total concentration of 7.5 μM in acetonitrile.

5. Binding constant plot

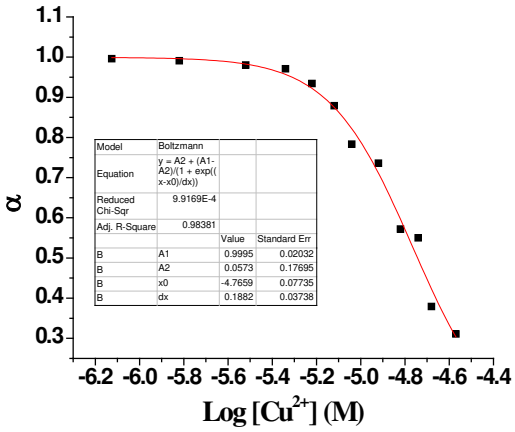

Cu(II)- ML

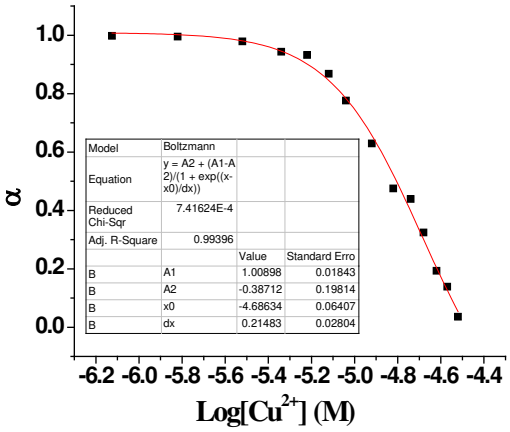

Cu(II)-AB2G1-L

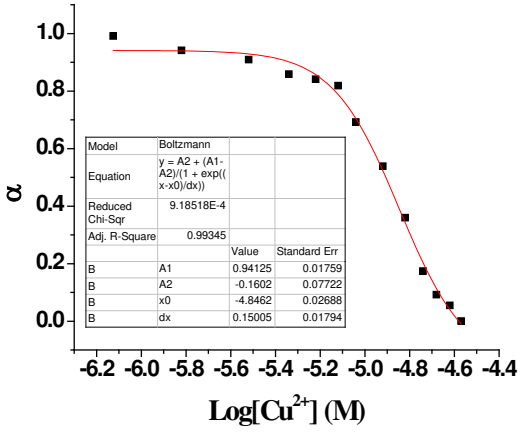

Cu(II)-AB2G2-L

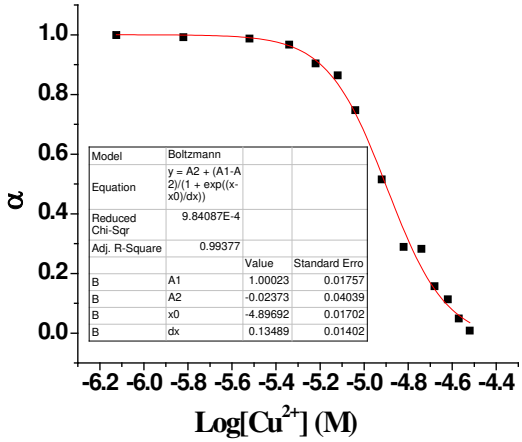

Cu(II)- AB3G2-L

Figure S5: Plot of α vs log [Cu^{2+}] for ML, AB2G1-L, AB2G2-L, AB3G2-L.

6. Fluorescence decay of the compounds Cu(II) complex of ML, AB2G1-L, AB2G2-L and AB3G2-L

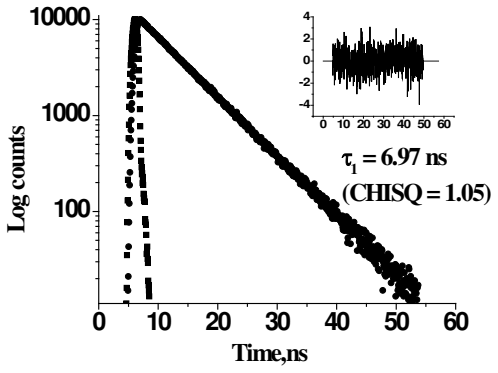

Cu(II)-ML

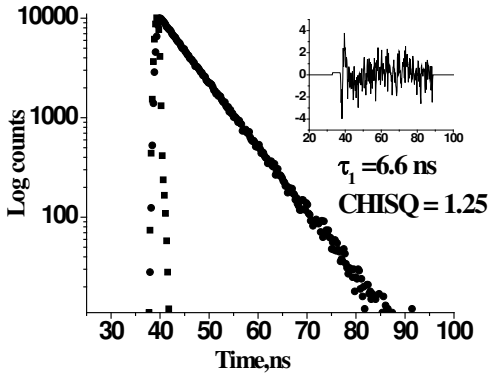

Cu(II)-AB2G1-L

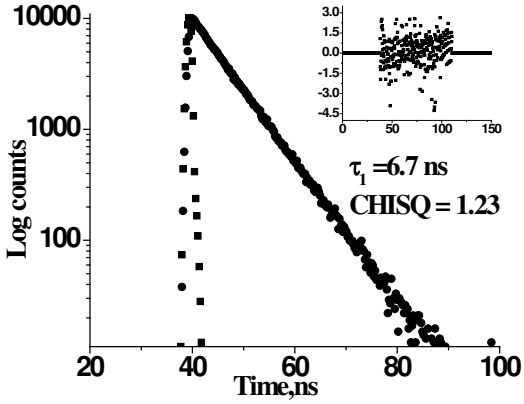

Cu(II)-AB2G2-L

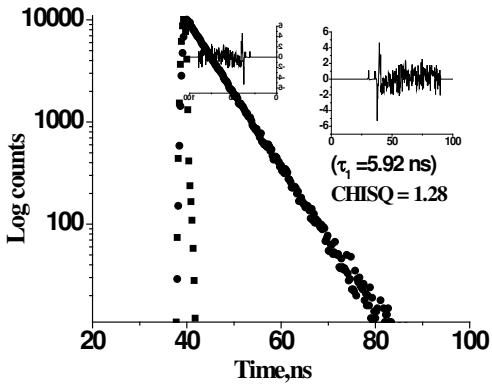

Cu(II)-AB3G2-L

Figure S6: Excited state decay from Cu^{2+}-ML, Cu^{2+}-AB2G1-L, Cu^{2+}-AB3G1-L, AB2G2-L and Cu^{2+}-AB3G2-L (7.5μM) in acetonitrile. λ_{ex} was 370 nm and emission was collected at 480 nm.

7. Steady state fluorescence spectra with respect to copper counter ion

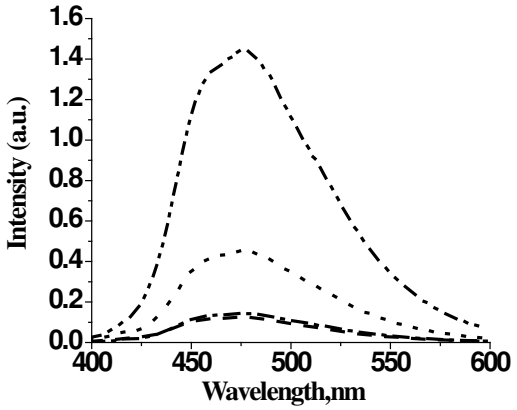

Cu(II)-ML

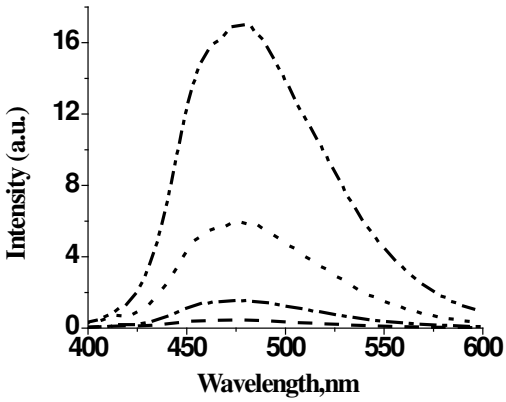

Cu(II)-AB2G1-L

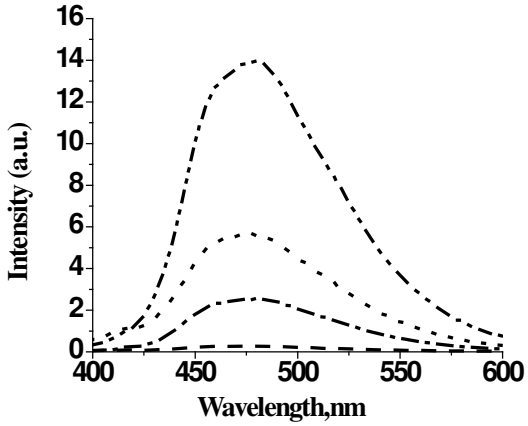

Cu(II)-AB2G2-L

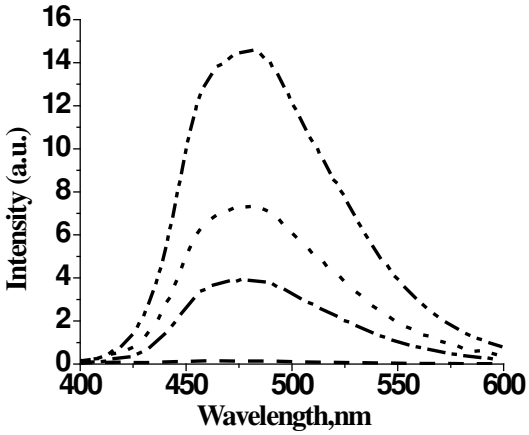

Cu(II)-AB3G2-L

Figure S7: The steady state emission spectra of ML,AB2G1-L, AB3G1-L, AB2G2-L and AB3G2-L (7.5μM) in acetonitrile in presence of $Cu(OAc)_2$ (dash), $Cu(Cl)_2$ (dash dot), $Cu(ClO)_4$ (dot), and $Cu(NO_3)_2$ (dash dot dot) (7.5μM) in acetonitrile. λ_{ex} was 370 nm.

8. Detection limit

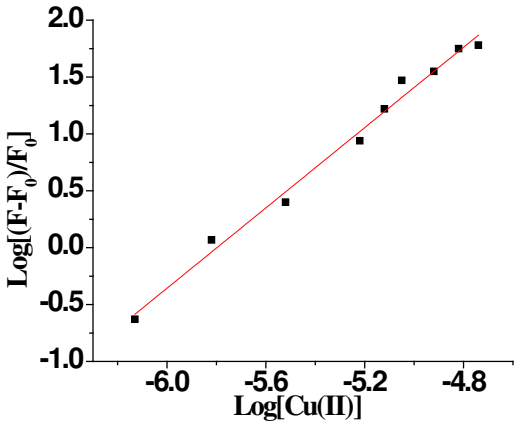

Cu(II)-ML

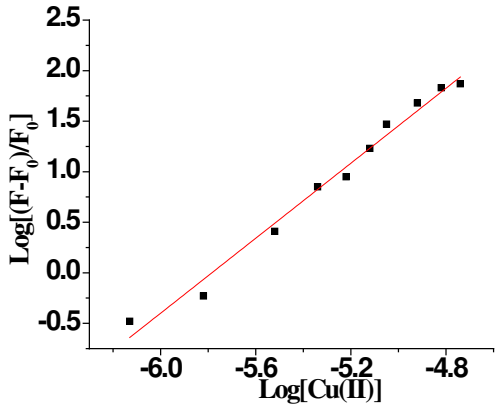

Cu(II)-AB2G1-L

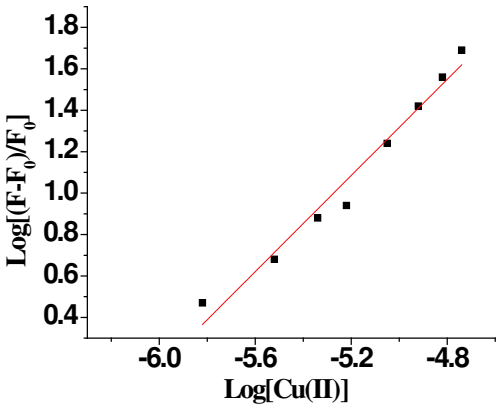

Cu(II)-AB2G2-L

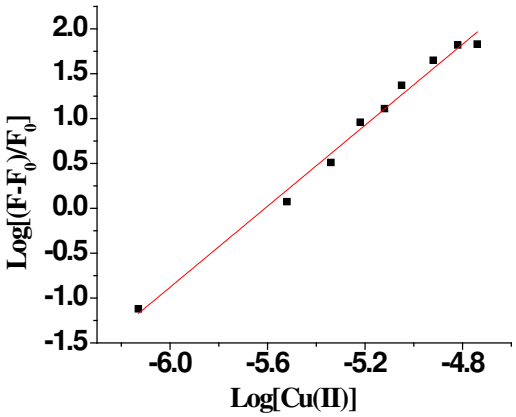

Cu(II)-AB3G2-L

Figure S8: Plot of intensity of ML, AB2G1-L, AB3G1-L, AB2G2-L and AB3G2-L (7.5μM) with respect to Cu(II) (0.75-18μM). λ_{ex} was 370 nm.

9. Photophysical study of Cu(II) complex of ML and AB3G1-L (7.5µM) in presence of other gases

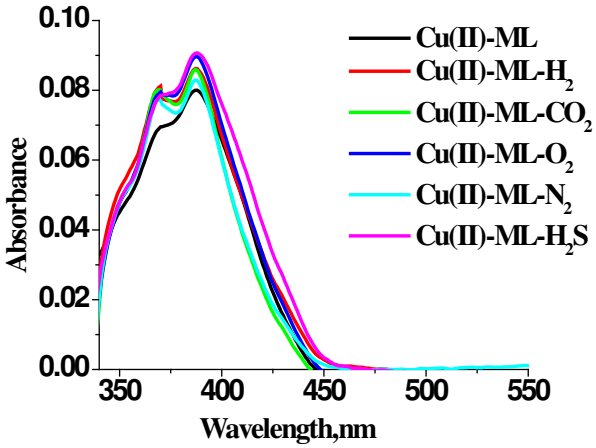

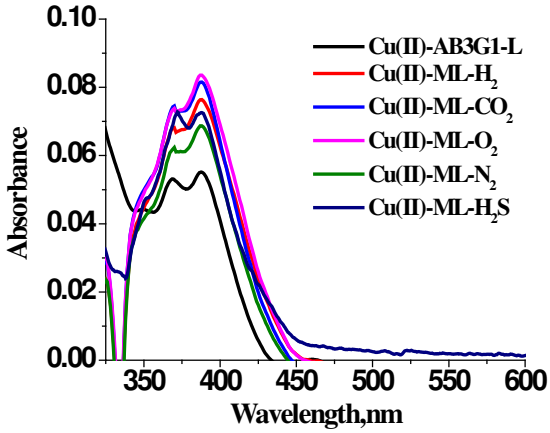

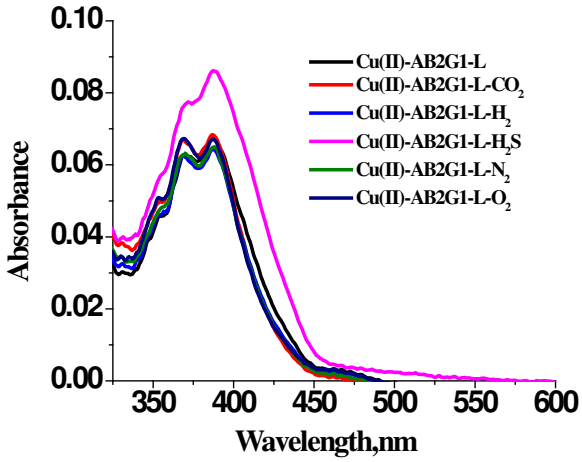

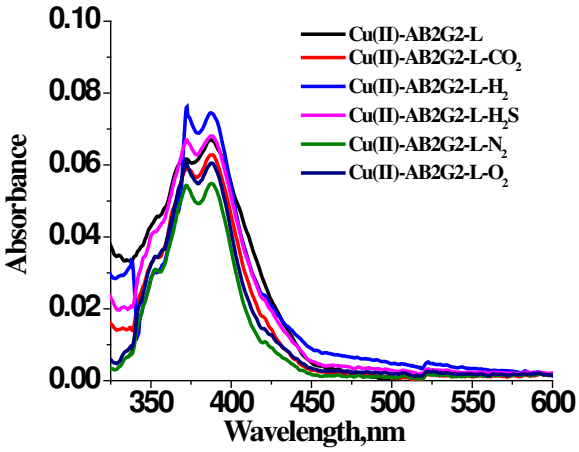

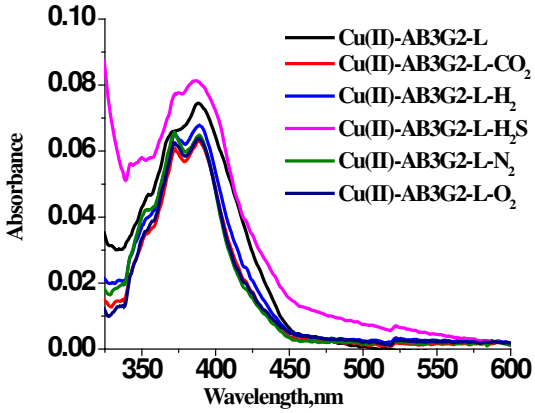

Figure S9: UV-Visible plot of Cu(II) complex of ML, AB3G1-L, AB2G1-L, AB2G2-L and AB3G2-L (7.5µM) upon passing of various gases for 15 minutes. λ_{ex} was 370 nm.

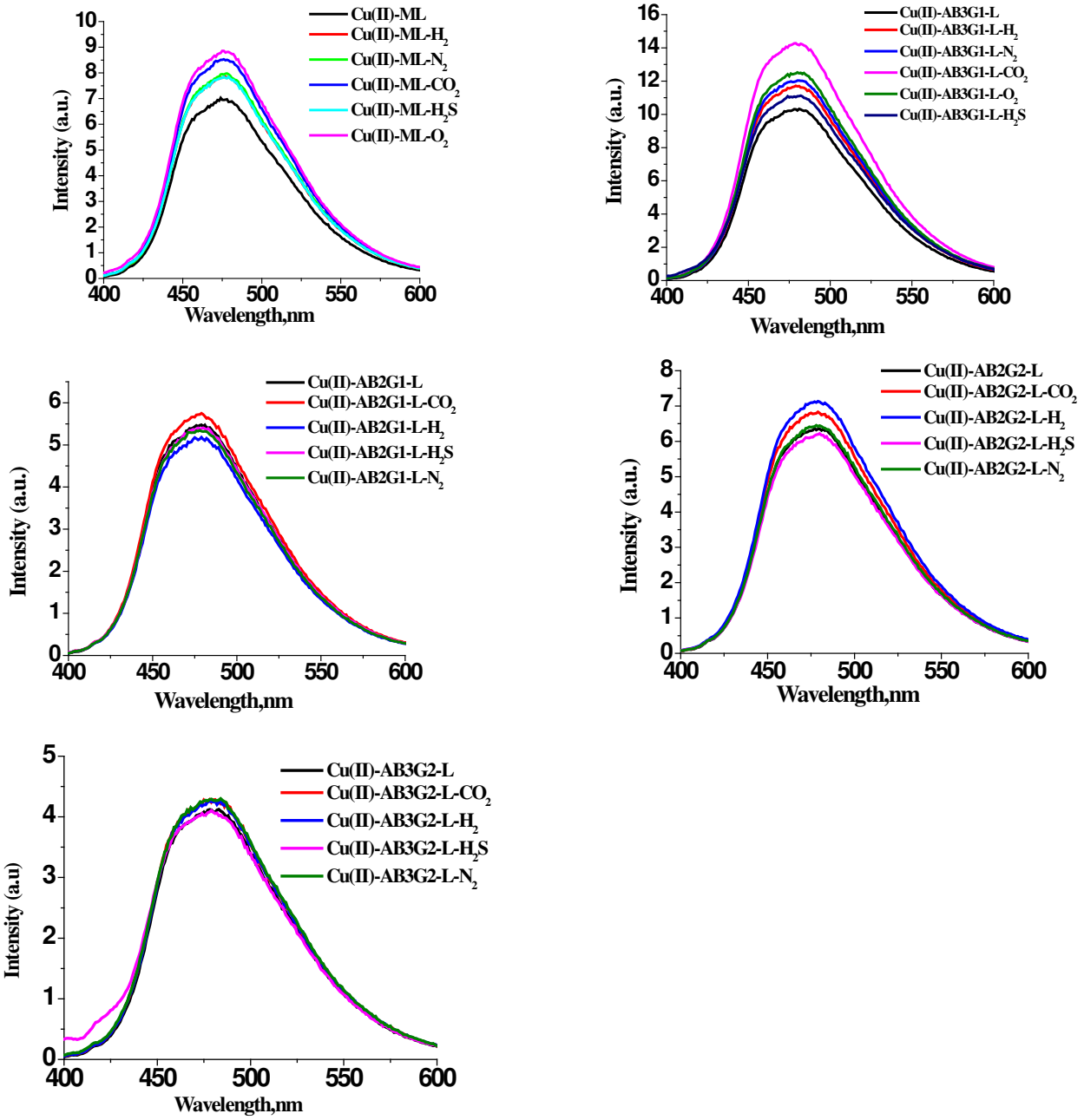

Figure S10: The steady state fluorescence spectra of Cu(II) complex of ML, AB3G1-L, AB2G1-L, AB2G2-L and AB3G2-L (7.5µM) upon passing of various gases for 15 minutes. λ_{ex} was 370 nm.

10. UV-visible absorption spectra of complex of Cu(II) with ML, AB2G1-L, AB3G1-L, AB2G2-L and AB3G2-L in presence of NO

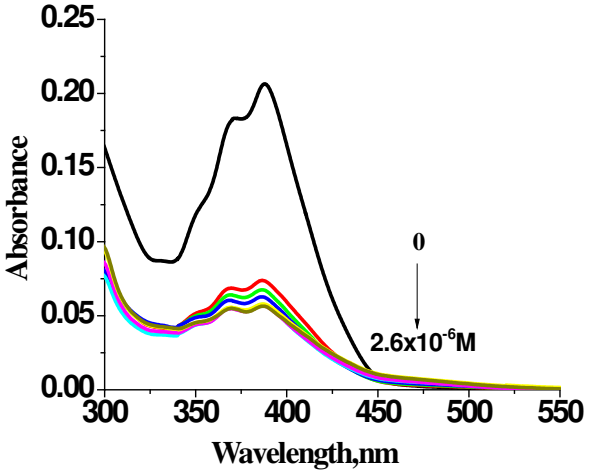

Cu(II)-ML-NO

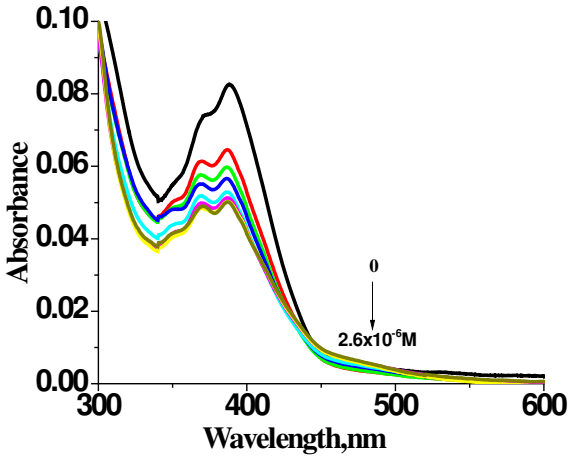

Cu(II)-AB2G1-L-NO

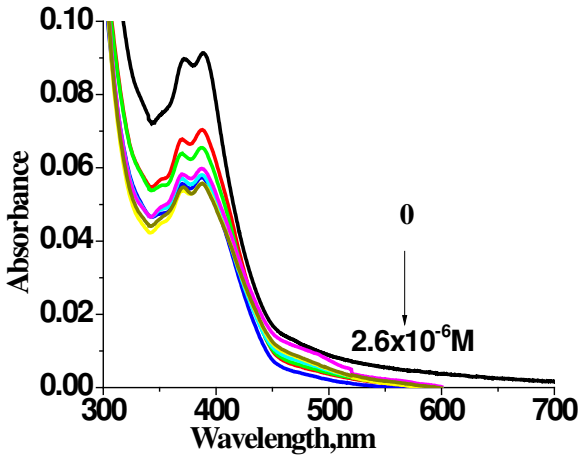

Cu(II)-AB2G2-L-NO

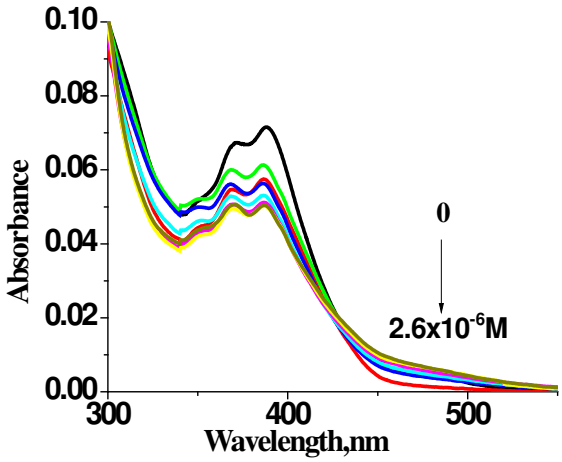

Cu(II)-AB3G2-L-NO

Figure S11: Absorption spectra of Cu(II) complex of ML, AB2G1-L, AB2G2-L and AB3G2-L (7.5μM) in acetonitrile in presence of NO (0-2.6μM).

11. Steady state fluorescence spectra of complex of Cu(II) with ML, AB2G1-L, AB3G1-L, AB2G2-L and AB3G2-L in presence of NO

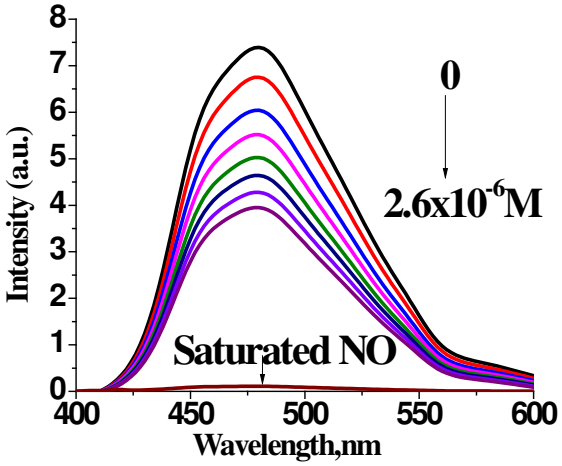

Cu(II)-ML-NO

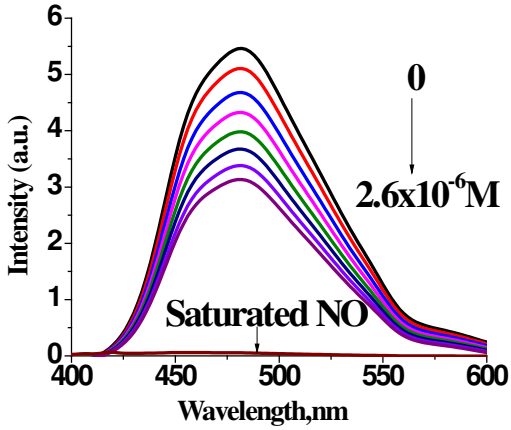

Cu(II)-AB2G1-L-NO

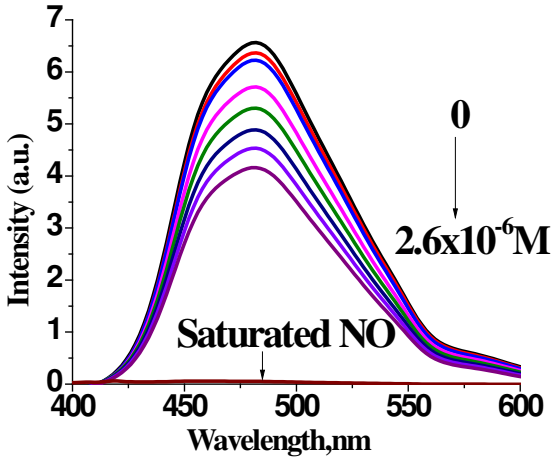

Cu(II)-AB2G2-L-NO

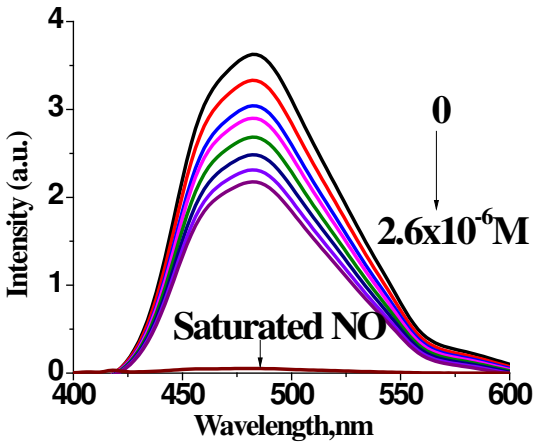

Cu(II)-AB3G2-L-NO

Figure S12: Emission spectra of Cu(II) complex of ML, AB2G1-L, AB2G2-L and AB3G2-L (7.5μM) in acetonitrile in presence of NO (0-2.6μM). λ_{ex} was 370 nm.

12. Stern-Volmer plot

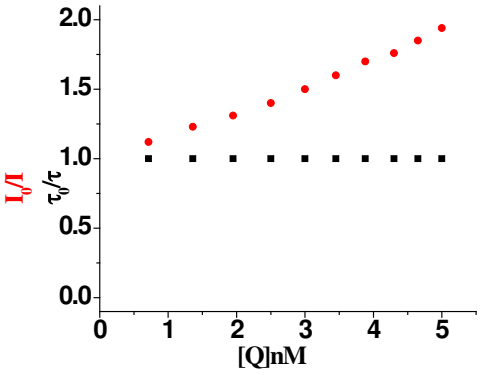

Cu(II)-ML-NO

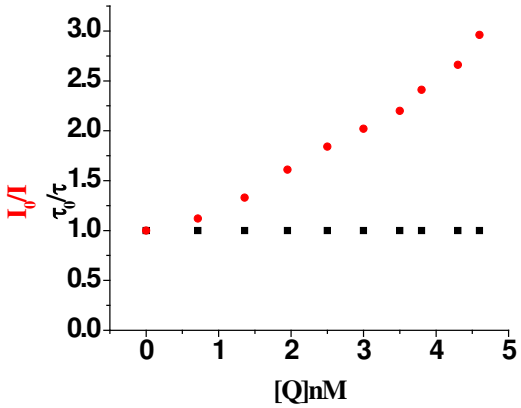

Cu(II)-AB2G1-L-NO

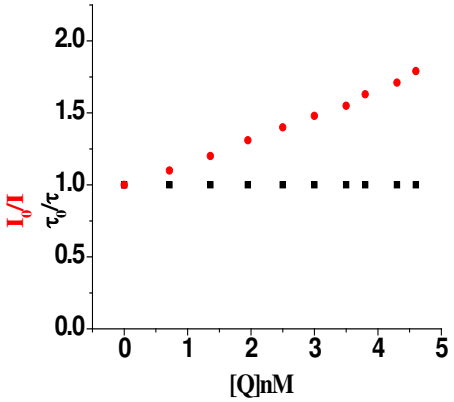

Cu(II)-AB2G2-L-NO

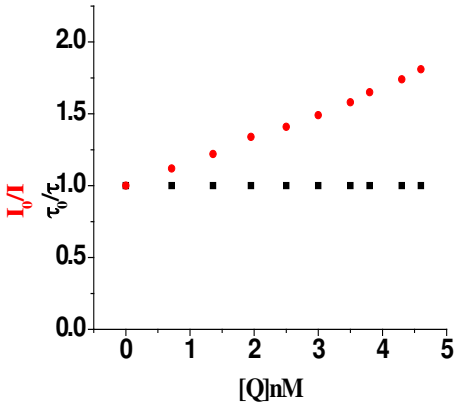

Cu(II)-AB3G2-L-NO

Figure S13: Stern-Volmer plot for the fluorescence quenching of Cu(II) complex of ML, AB2G1-L, AB2G2-L and AB3G2-L (7.5µM) upon addition of NO (0.7nM-0.5nM) in acetonitrile. λ_{ex} was 370 nm.

13. EPR of complex of Cu(II) with ML, AB2G1-L, AB3G1-L, AB2G2-L and AB3G2-L in presence and absence of NO

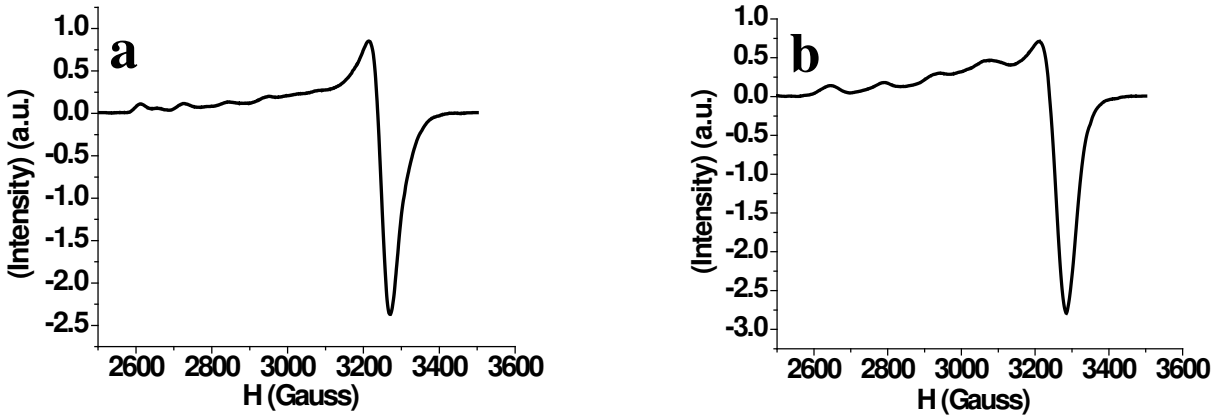

Figure S14a: X band EPR spectrum of ML complex of Cu(II) in absence (a) and presence (b) of NO in acetonitrile at 77K.

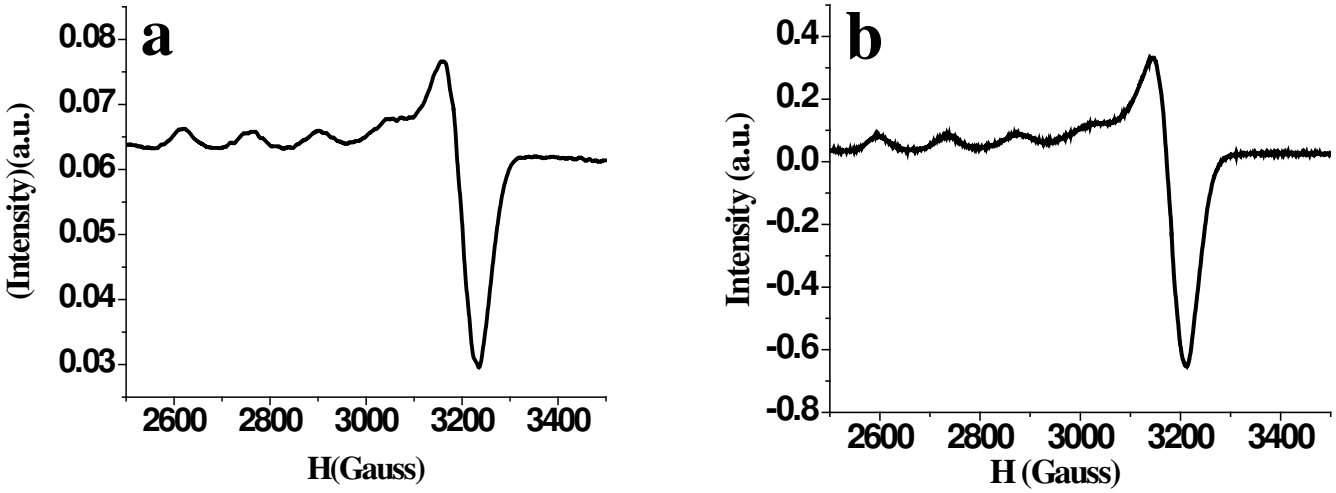

Figure S14b: X band EPR spectrum of AB2G1-L complex of Cu(II) in absence (a) and presence (b) of NO in acetonitrile at 77K.

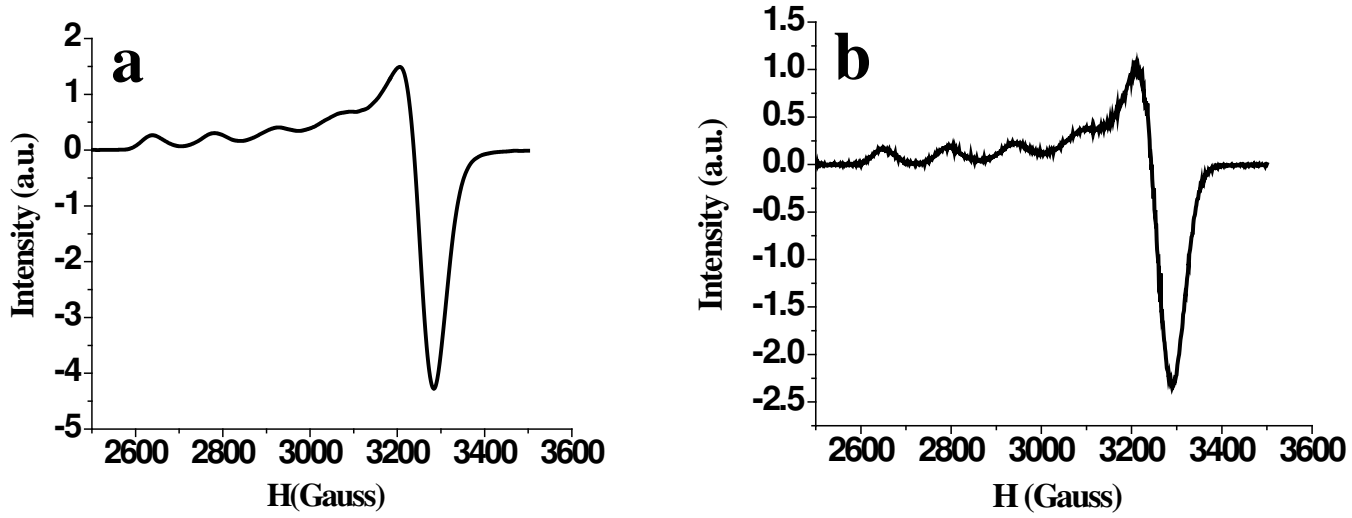

Figure S14c: X band EPR spectrum of AB3G1-L complex of Cu(II) in absence (a) and presence (b) of NO in acetonitrile at 77K.

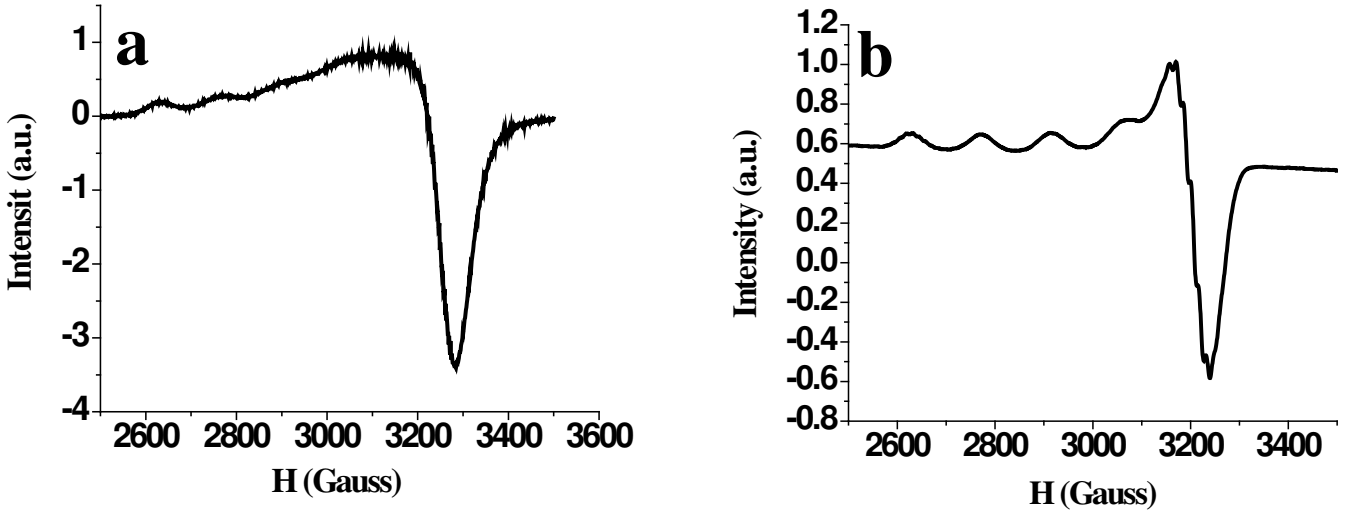

Figure S14d: X band EPR spectrum of AB2G2-L complex of Cu(II) in absence (a) and presence (b) of NO in acetonitrile at 77K.

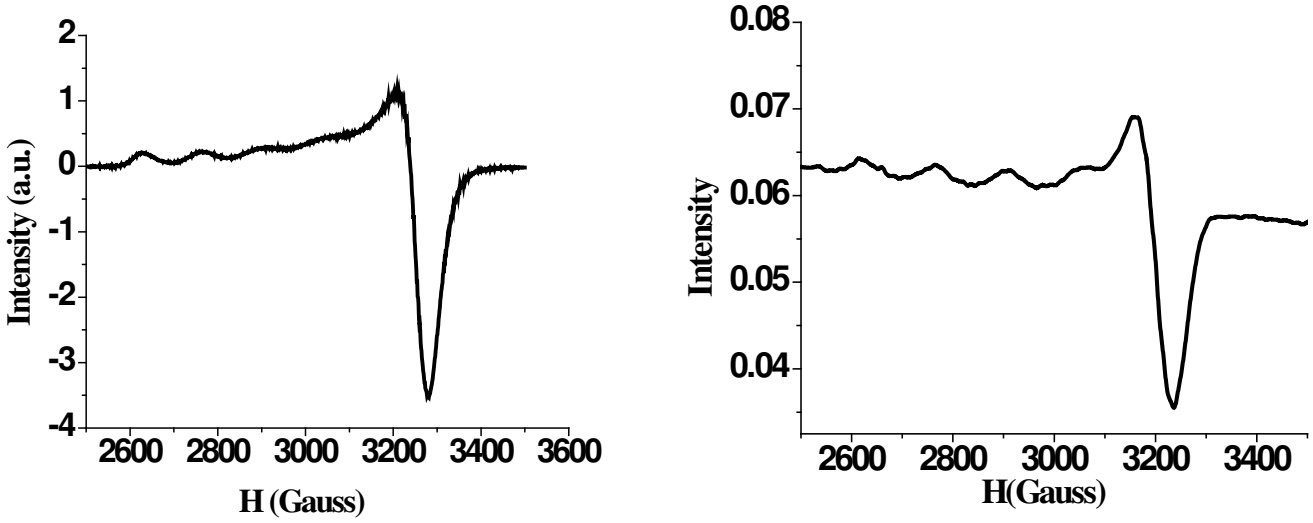

Figure S14e: X band EPR spectrum of AB3G2-L complex of Cu(II) in absence (a) and presence (b) of NO in acetonitrile at 77K.

14. FT-IR data

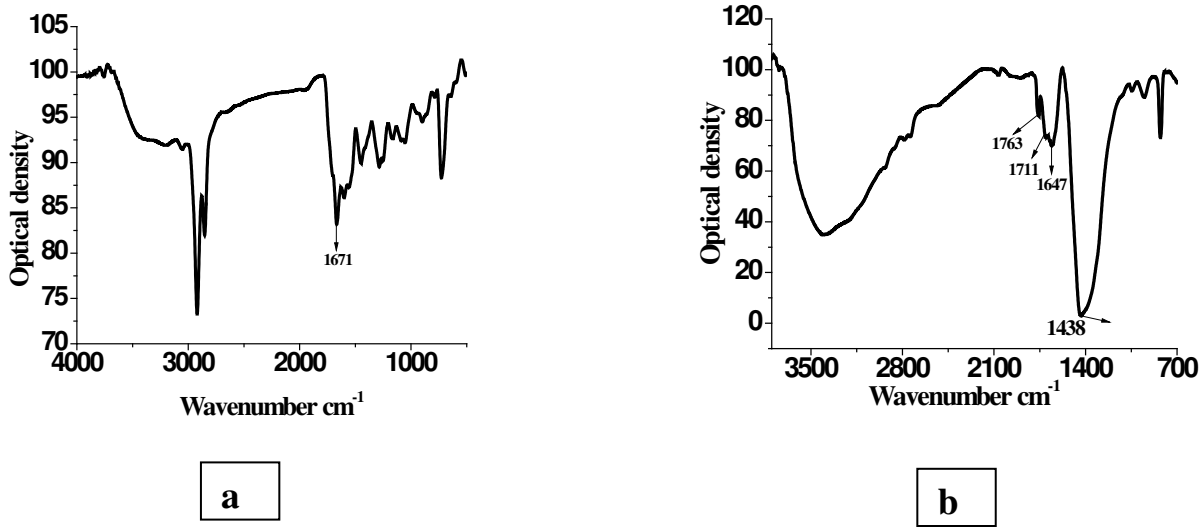

Figure S15a: Solution FTIR spectrum of Cu(II) - ML complex in the absence (a) and presence of NO (b) in acetonitrile.

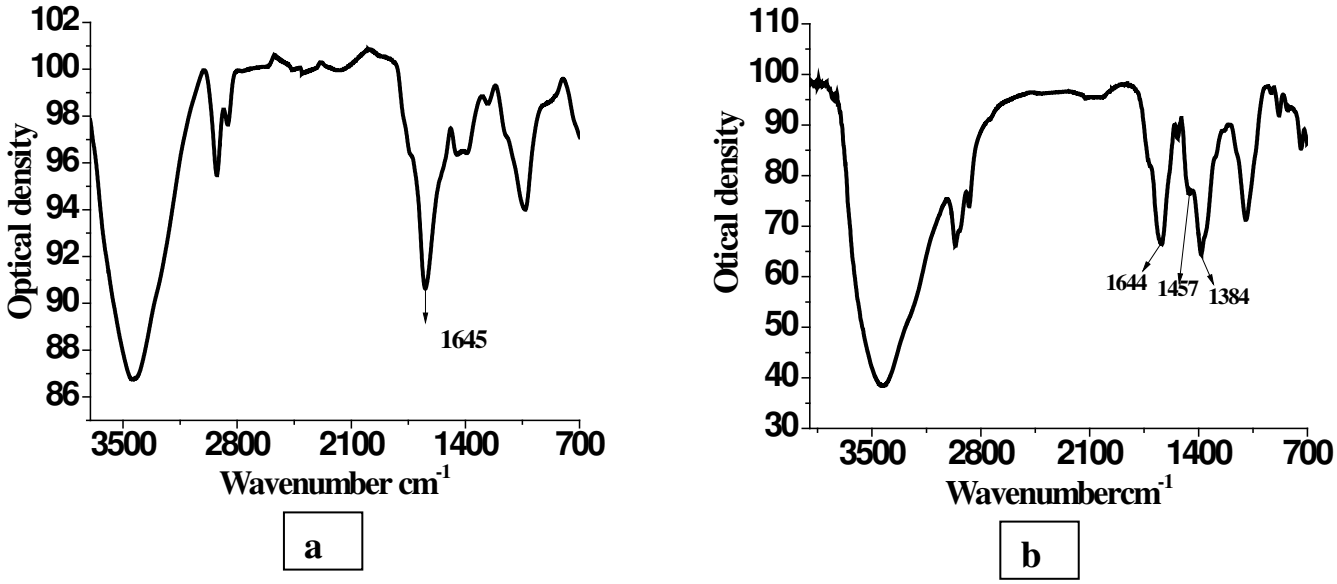

Figure S15b: Solution FTIR spectrum of Cu(II)-AB2G1-L complex in absence (a) and presence of saturated NO (b).

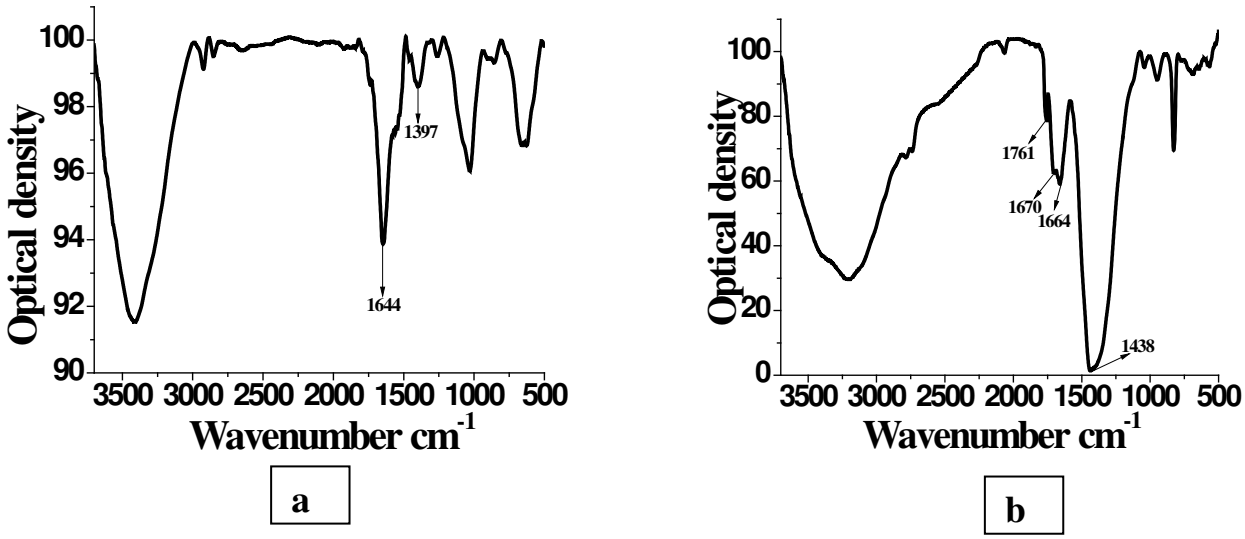

Figure S15c: Solution FTIR spectrum of Cu(II)-AB3G1-L complex in absence (a) and presence of saturated NO (b) in acetonitrile.

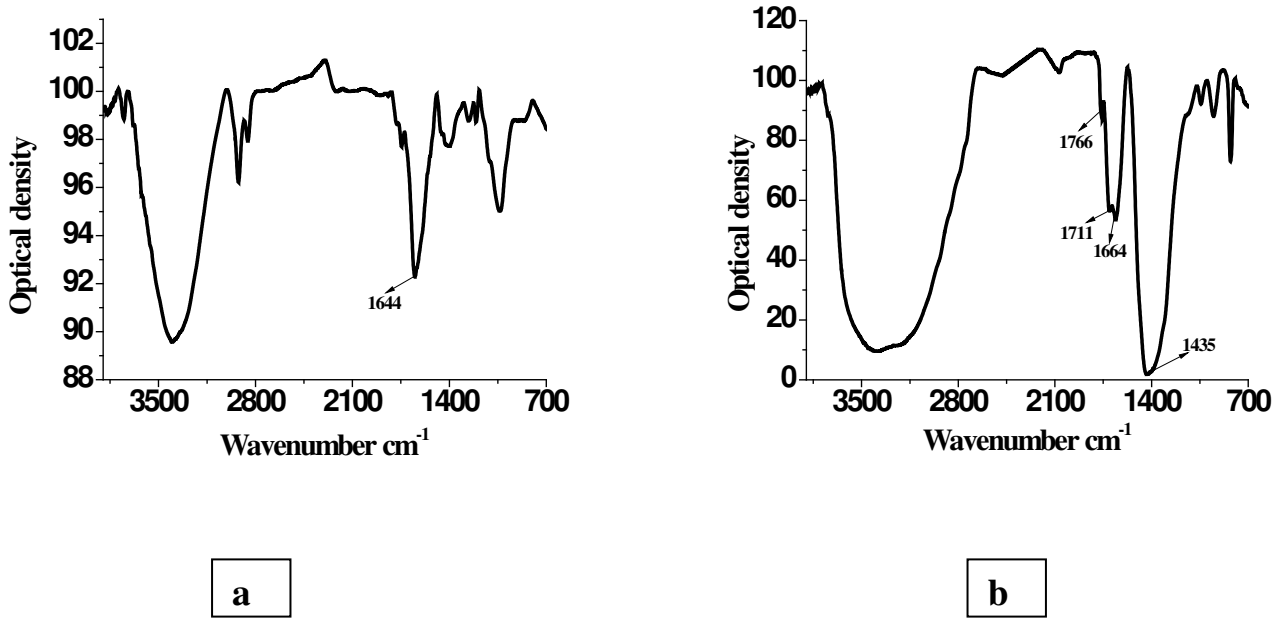

Figure S15d: Solution FTIR spectrum of Cu(II)-AB2G2-L complex in absence (a) and presence of saturated NO (b) in acetonitrile.

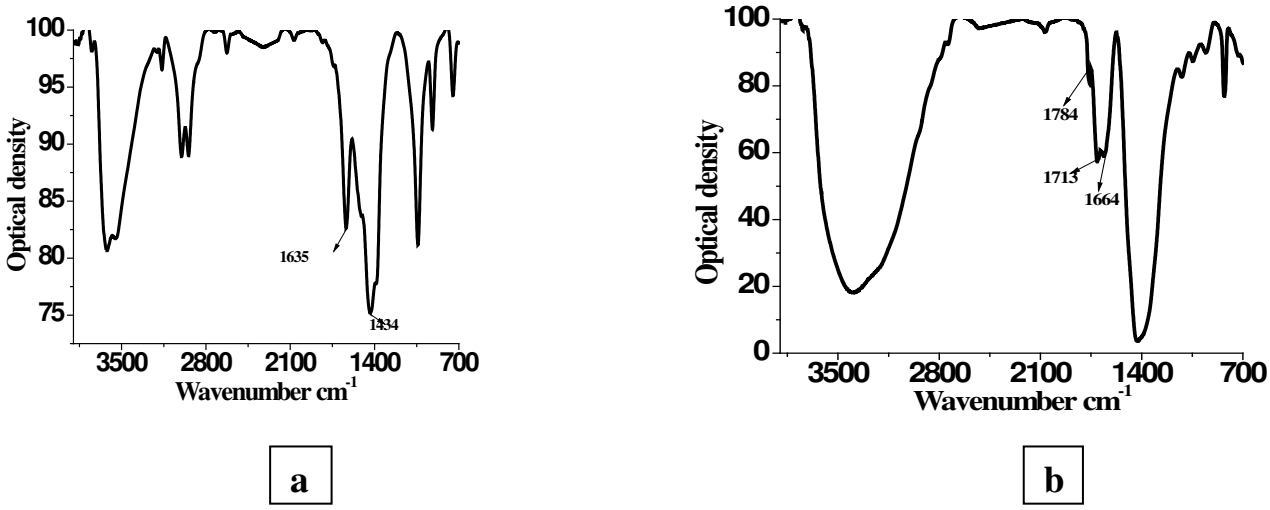

Figure S15e: Solution FTIR spectrum of Cu(II)-AB3G2-L complex in absence (a) and presence of saturated NO (b) in acetonitrile.